Flood attenuation hydraulics of channel-spanning leaky barriers

Valentine Muhawenimana[a], Catherine A.M.E. Wilson[a], Jelena Nefjodova[b], and Jo Cable[b]

[a] Cardiff School of Engineering, Cardiff University, Cardiff, CF24 3AA, UK

[b] Cardiff School of Biosciences, Cardiff University, Cardiff, CF10 3AX, UK

Corresponding author: Valentine Muhawenimana (MuhawenimanaV@cardiff.ac.uk)

Abstract

Natural flood management aims to enhance natural processes to build resilience into flood risk management alongside hard engineering methods of flood defence, using 'soft engineering' methods such as leaky barriers. This study addresses the research gaps pertaining to the backwater effects of different leaky barrier designs and the physical characteristics that determine the extent of flood attenuation. Porous and non-porous leaky barrier designs, which varied by longitudinal length, blockage ratio, mode of formation and log arrangement, were tested in a laboratory flume with a compound channel cross-section. Flow area afflux (defined as the upstream increase in flow area caused by the leaky barrier compared to the uniform flow condition without the barrier) and headloss were used to quantify the backwater effects of the leaky barrier under 80 and 100% bankfull discharges. For inbank flows, leaky barrier longitudinal length and cross-sectional blockage ratio governed head loss and drag coefficients, which were higher for non-porous than for porous leaky barriers. The cross-sectional blockage ratio was the primary factor increasing area afflux, indicating that leaky barrier designs which maximise channel obstruction will result in higher flood attenuation. Streamwise length had a limited effect on stage and area afflux,

unless it was accompanied by an increase in blockage ratio, especially for the non-porous structures. The use of uniformly distributed logs resulted in equal or higher area afflux than the more physically complex barriers that used varied log orientations. The non-porous structures resulted in at least twice the area afflux compared to their porous counterparts, indicating that over time, accumulation of organic matter and sediments, which render the barriers more watertight, will enhance backwater effects, flood storage and downstream attenuation.

Keywords: Flooding; Backwater; Natural flood management; Leaky barrier; Woody debris; flood attenuation

Highlights

- Experiments tested leaky barriers varying by longitudinal length and blockage ratio
- Barriers raised the upstream flow area by 0 to 30% of the uniform flow condition
- Non-porous barriers resulted in at least twice the flow area afflux of porous dams
- Cross-sectional blockage ratio parameter primarily maximised flood attenuation

1. Introduction

Flooding is one of the most devastating and costly natural disasters (UNISDR 2015). In this era of 'global weirding', globalization and urbanisation, flood risk management has ever increasing importance to reduce human suffering and economic loss (Carrera et al. 2015; UNISDR 2015; Pellicani 2018). To meet this challenge, flood management has switched from defence to risk strategy (Fleming 2002; Pitt 2008; Carrera et al. 2015; UNISDR 2015). Current solutions use hard engineering measures such as flood walls, channel widening, flood storage reservoirs, by-pass channels and flood gates, as well as the use of temporary barriers, but also new 'soft engineering' solutions in the form of Natural Flood

48 Management (NFM) in an effort to build resilience into traditional methods (Pitt 2008;
49 SEPA 2015; Burgess-Gamble et al. 2017; Dadson et al. 2017). NFM is a relatively new
50 field that uses natural processes at a catchment scale, to reduce runoff, increase ground
51 infiltration, increase floodplain storage and reduce river velocity, which includes measures
52 such as earth bunds, ditches and storage ponds, leaky barriers and woodland planting
53 (Nisbet et al. 2011; SEPA 2015; Burgess-Gamble et al. 2017). Perhaps one of the most
54 cost-effective measures is the introduction of leaky barriers in middle and upper catchments
55 that attenuate flood processes by diverting flow onto floodplains (Fig. 1). The resulting
56 backwater effect enhances floodplain storage and increases ground infiltration, thereby
57 attenuating surface flows and slowing down flooding downstream (Gippel 1995; Thomas
58 and Nisbet 2012; Quinn et al. 2013).
59 Manmade, engineered leaky barriers are designed to imitate beaver dams, which impound
60 rivers and can retain large volumes of water (Nyssen et al. 2011; Wohl 2013; Giriat et al.
61 2016; Puttock et al. 2017), and log jams or woody debris dams, which are naturally
62 occurring woody debris accumulations of trees and branches recruited from river banks
63 that partially or fully obstruct flow (Wallerstein and Thorne 1997; Abbe and Montgomery
64 1996; Manners et al. 2007; Dixon and Sear 2014). In naturally occurring leaky barriers, key
65 components act as support structures for the entire barrier, and smaller diameter and shorter
66 length branches accumulate behind the key members (Wallerstein and Thorne 1997;
67 Manners et al. 2007; Schalko et al. 2019). River management and restoration schemes have
68 a complex history whereby woody debris were removed from rivers to improve navigation
69 or to reduce channel resistance as they were believed to increase flood risk (Young 1991;
70 Gippel et al. 1992; Shields and Gippel 1995). This, however, was prior to the recognition
71 that woody accumulations enhance natural processes and help to restore deteriorating
72 fluvial habitats, by providing refugia and shade for fish, improving water quality, and

trapping sediment, organic matter and nutrients (Gippel 1995; Gippel et al. 1996; Roni et al. 2015; SEPA 2015).

Pilot studies have shown that channel spanning leaky barriers can provide flood alleviation by delaying the flood peak and increasing flood travel time (Gregory et al. 1985; Wenzel et al. 2014; Burgess-Gamble et al. 2017; Dadson et al. 2017) (Illustrated in Fig. 1). Hydraulic models in particular, use a hydraulic roughness coefficient to model and calibrate the flow-obstructing nature of leaky barriers (Kitts 2010; Odoni and Lane 2010; Thomas and Nisbet 2012) even though the intended use of a roughness coefficient is to represent the resistance to flow applied by the bed, bank and floodplain boundary material (Chow 1959). Furthermore, previous research on woody debris accumulations has focused on the removal of woody material in river management, rather than the capacity for natural flood management (Gippel et al. 1992; Shields and Gippel 1995; Manners et al. 2007).

Much remains unknown on the hydraulic changes that channel-spanning leaky barriers make to flow processes by altering the upstream surface water profile, constricting and diverting flow, and attenuating flow. Experimental studies of channel spanning leaky barriers have assessed the effects of single woody elements (Young 1991). But this does not accurately represent the hydraulic complexity of flows through natural and engineered leaky barriers, which are composed of multiple timbers (Daniels and Rhoads 2007; Manners et al. 2007; Schalko et al. 2018; Schalko et al. 2019). The process and extent of these benefits have yet to be effectively quantified; there is currently limited evidence for leaky barrier design and flood attenuation performance (Burgess-Gamble et al. 2017).

Here, we experimentally quantified the backwater flow area rise, head loss and flood attenuation performance of full-span leaky barriers in relation to the barriers' streamwise length, cross-sectional blockage area, height in the water column, orientation and angle of the timbers and barrier configuration, for porous and non-porous conditions. These were

tested in an open channel flume for two flow conditions, bankfull (100% bankfull) and near bankfull (80% bankfull) conditions. Quantitative analysis of the backwater effects of these leaky barriers allowed us to provide recommendations of key physical attributes for optimising their performance.

2. Methodology

2.1. Flume and uniform flow conditions

Experiments were conducted in an open channel recirculating flume 10 m long, 1.2 m wide, and 0.3 m deep (L_{flume}, B_{flume}, H_{flume}) set to a 1/1000 bed slope. PVC sheets partitioned the flume into a symmetric compound channel, with a rectangular main channel of width 0.6 m (B_{mc}) and total floodplain width (B_{fp}) of 0.6 m comprised of two 0.3 m wide floodplains on each side of the main channel. The main channel had a bankfull depth of 0.15 m (Fig. 2A and B). A pump with 0.6 m^3s^{-1} capacity recirculated the water and controlled the discharge, while a sharp crested tailgate weir located at the downstream end of the flume maintained the surface water profile along the flume. An ultrasonic flow meter (TecFluid Nixon CU100) measured the discharge to a precision of ± 1.5%. A Vernier pointer gauge was used to measure the flow depth (±0.2 mm). Prior to installation of the leaky barrier, uniform flow conditions were established for 80% bankfull flow condition ($0.8Q_{bk}$) and 100% bankfull flow condition (Q_{bk}), relating to discharges (Q) of 0.22 and 0.28 m^3s^{-1} and uniform flow depths h_0 of 0.13 and 0.15 m, respectively (Table 1). Reynolds numbers $Re = U_0R_0/\nu$, (where the hydraulic radius $R_0 = B_{mc} * h_o/(B_{mc}+2h_o)$ and kinematic viscosity $\nu = 1*10^{-6}$ m^2s^{-1} for water temperature = 20°C) were 25,600 for $0.8Q_{bk}$ and 31,100 for $Q_{bk.}$. These flow conditions relate to subcritical conditions ($Fr < 1$, the Froude number $Fr = U_0(gh)^{-0.5}$, where g is the gravity acceleration) and were used throughout all experiments. Subscripts

mc and fp refer to the main channel and floodplain respectively, while 1 and 2 refer to cross-sections upstream and downstream of the leaky barrier respectively (Fig. 2A).

2.2. Leaky barrier arrangements

Geometrically arranged leaky barriers were tested through a series of experiments for $0.8Q_{bk}$ and Q_{bk} discharges: Linear (Li), Lattice (La), and Alternating (AL) (see Fig. 2). The barriers were constructed using wooden dowels fixed to the sides of the main channel using silicone adhesive, with each barrier spanning the full width of the main channel.

The geometric arrangements of the Linear barriers consisted of arrays of constant diameter (25 mm) horizontal logs spanning the full main channel width. The height of Linear barriers, H_s, was the elevation from the top log's edge to the bottom log (Fig. 2), corresponding to the use of 1, 2 or 3 rows of logs in the leaky barrier array (test series A1-A8 and A25-A32, A9-A16 and A33-A40, A17-A24, A41-A48, respectively). Lattice arrangements were comprised of logs orientated diagonally at an angle of 6^{o} to the horizontal (test series B1-B8). Alternating barriers were a hybrid of the Linear and Lattice barriers, where dowels alternated between a layer of horizontally orientated dowels followed by a layer of the inclined dowels (test series C1-C8).

All logs comprising the barrier were oriented perpendicular to the flow. A vertical gap (b_0) of 50 mm, one third of the main channel depth, between the barrier's lowest log and the channel bed was maintained throughout all the leaky barrier experiments. In previous studies this unoccupied gap between the riverbed and the barrier serves to allow low flows to pass unobstructed through the channel and to allow the free movement and passage of fish (Nisbet et al. 2011; SEPA 2015; Dodd et al. 2016). For the Linear, Lattice, and Alternating arrangements, the barrier length (L_x) in the longitudinal flow direction (XY plane) was increased by consecutively adding a layer of logs along the channel in the YZ plane (Fig. 3). Details of the barrier arrangements are given in Table 1 and Figure 2.

Finally, for the Linear arrangements (test series A25-A348), we tested a non-porous leaky barrier by wrapping the porous barrier in plastic film, rendering it impermeable, emulating the natural clogging and accumulation of sediment, leaves, small branches and other debris immediately behind the barrier to form a solid non-porous body. When this occurs naturally, the organic material accumulation decreases water flow paths through the barrier until it becomes completely saturated and more watertight (Manners et al. 2007; Schalko et al. 2018; Schalko et al. 2019). Non-porous cases were trialled for the Lattice and Alternating arrangements, however, due to the inclined logs not fully supporting the plastic film, it caved in above and below the barrier as it filled with water, and hence these data were not included in the analysis.

The flow cross-sectional blockage ratio A_B (-), hereafter referred to as blockage ratio, was defined by the proportion of the flow cross-sectional area occupied by the barrier:

$$A_B = \frac{A_p}{A} \quad (1)$$

Where the cross-sectional frontal projected area of the logs $A_p = \sum a_p$ with a_p as the projected area of each log, and the flow cross-sectional area $A = B_{mc} * h_0$, B_{mc} as the main channel width and h_0 as the uniform flow depth.

2.3. Stage measurements, head loss and drag coefficients

Water surface profiles were measured along the main channel centreline using a Vernier pointer gauge (nearest 0.1 mm) from a distance of 2 m from the upstream inlet until a distance 8 m from the inlet (2 m upstream of the downstream weir). The spatial resolution of the water surface level measurements in the longitudinal flow direction was such that spacing between measurements ranged from 2 mm to 500 mm, with higher spatial resolution measurements in the vicinity of the leaky barrier, located 5 m from the flume inlet. Spatial fluctuations in the surface water level in the proximity of the barrier were not

included in the calculations of mean flow depth. Spatially-averaged measurements of flow depth upstream (h_1), from the flume inlet, 3 to 4.68 m, and downstream (h_2) 5.5 to 6.5 m (Fig. 4) were used for calculating the stage afflux (Δh), and upstream flow area afflux rise (ΔA), which are given by:

$$\Delta h = h_1 - h_0 \quad (2)$$

and

$$\Delta A = A_1 - A_0 \quad (3)$$

Where A_1 is the upstream flow area and A_0 is the uniform flow cross section. These parameters were normalised by the uniform flow depth and flow area to obtain $\Delta h/h_0$ and $\Delta A/A_0$, respectively. A volumetric approach to characterise the backwater effect of the leaky barriers was adopted to comparatively evaluate the flow area afflux including the overbank flows on the floodplains, which due to the compound channel section would not be adequately represented by an approach based solely on flow depth.

For inbank flow depths of the 80% bankfull flow condition, the head loss (h_L) was calculated using the Energy equation, where total energy head (H) in m is:

$$H = z + h + \frac{{U_0}^2}{2g} \quad (4)$$

And head loss is:

$$h_L = \Delta H = H_1 - H_2 = \left(\frac{U_1^2}{2g} + \overline{h_1}\right) - \left(\frac{U_2^2}{2g} + \overline{h_2}\right) \quad (5)$$

Where z is the flume bed elevation, h is the flow depth, U_0 is the cross-sectional average velocity, $U_1 = \frac{Q}{\overline{h_1} * B_{mc}}$ and $U_2 = \frac{Q}{\overline{h_2} * B_{mc}}$ are the upstream and downstream cross-sectional average velocities respectively. Subscripts 1 and 2 refer to upstream and downstream sections from the dam.

Empirical formulae for stage rise Δh based on the momentum principle and modelling leaky barriers as cylindrical obstructions, given by Ranga Raju et al. (1983) and Gippel et al. (1996) is used to calculate the drag coefficient directly from the measured stage afflux:

$$\Delta h = \frac{1}{3}h\{(F_{r2}^2 - 1) + [(F_{r2}^2 - 1)^2 + 3C_D A_B F_{r2}^2]^{0.5}\} \quad (6)$$

Where the Froude number downstream of the leaky barrier is $F_{r2} = \frac{U_2}{(gh_2)^{0.5}}$, U_2 is the mean velocity downstream of the leaky barrier, h_2 is the downstream mean flow depth, and the blockage ratio A_B is as shown in Eq. 1.

3. Results

3.1. Longitudinal water surface profiles

Longitudinal water surface profiles for Linear case for porous (test series A1 to A24) and non-porous (test series A25 to A48) conditions are shown in Figure 3, in comparison to the uniform flow condition without the barrier. The Linear case is presented here for brevity, but the profiles were similar for all cases. As would be expected for flow around a submerged obstacle, the water surface elevation reaches its highest peak immediately upstream of the leaky barrier then declines over the leaky barrier's top before plummeting to its lowest elevation immediately downstream of the leaky barrier. The water surface remains stable approximately 50 cm upstream and downstream of the leaky barrier. The water surface profiles show the stage afflux due to the leaky barrier and the enhanced rise due to the "no through" non-porous barrier compared to its "flow through" porous counterpart (Fig. 3).

3.2. The Effect of the leaky barrier on inbank flow conditions

An increase in head loss was observed for all configurations with increasing L_x (Fig. 4A). However, for a given A_B results revealed that Linear barriers showed higher head loss than

Lattice. Alternating barriers showed higher head loss than Lattice, but similar to Linear barrier, depending on the height of the leaky barrier in the water column, even though Alternating had much higher A_B than other configurations for similar L_x values. For Linear cases, H_s = 95 mm (test series A9-A16), had a greater blockage ratio than H_s = 60 mm (test series A17-A24), resulting in about twice the headloss. Based on blockage ratio (Fig. 4B), the Linear barrier showed higher stage afflux than the Lattice (test series B1-B8) and Alternating barriers (test series C1-C8) for similar A_B values.

For Linear porous barriers with inbank flows, stage afflux $\Delta h/h_0$ was higher for 100% bankfull than for 80% bankfull discharges. As with headloss, due to greater cross-sectional blockage ratio H_s = 95 mm resulted in higher stage afflux than H_s = 60 mm. Overall, $\Delta h/h_0$ tended to increase with increasing volume of wood, barrier length and cross-sectional blockage ratio. Comparison with series A7 (Fr = 0.30) from Schalko et al. (2019), chosen to maintain Froude similarity with the current data, showed a similar trend and range of resulting stage afflux for a given relative leaky barrier relative solid volume, with differences likely due to variations in leaky barrier cross-sectional blockage ratio.

In terms of hydrodynamic drag, the drag coefficient C_D increased with longitudinal leaky barrier length for inbank flows for Linear barriers (Fig. 6A), and increased with cross-sectional blockage ratio A_B (Fig. 6B), consistently within the range of C_D values observed in previous studies; indicating that leaky barrier obstructions although porous result in drag coefficients similar to those of single branched and unbranched cylinder obstructions (Shields and Alonso 2012). The vertical scatter of C_D values for the same blockage ratio is attributed to the effect of the leaky barrier longitudinal length, which increased surface drag, and therefore C_D, as seen in the data distribution in Fig. 6A.

3.3. Effect of streamwise length, projected area and blockage ratio of the barrier on area afflux

The linear barrier configuration was used to evaluate how the distribution of logs in the cross-sectional (YZ plane) and longitudinal sectional (XZ plane) planes with increasing volumes of wood affect area afflux. With the exception of non-porous barrier with the highest blockage area relating to the barrier with the highest elevation log (H_s= 95 mm), an increase in the barrier's longitudinal length (L_x) resulted in minor increases in area afflux for the same H_s setting (Figs. 7A and B). Area afflux increased with increasing flow blockage ratio of the barrier, in general for the lower blockage ratio barriers when the barrier frontal projected area doubled the upstream flow area afflux doubled, and this effect became more enhanced with higher blockage area leaky barriers (H_s= 95 mm), a pattern that was observed for both 80% and 100% bankfull discharges (Figs. 7C and D). The non-porous barrier showed considerably higher area afflux than the porous structure (Figs. 7B and D).

Area afflux increased with increasing leaky barrier frontal projected area, corresponding to the increase in projected area of logs in the cross-sectional YZ plane and blockage ratio of the main channel cross-section (Figs. 7C and D). For the porous barriers, an increase of log volume in the longitudinal X direction (XZ plane) created by increasing the length of the barrier (L_x), resulted in minor increases in local losses, as the flow streamlined between the voids of the barrier. Amongst Linear barriers of the same cross-sectional blockage ratio, increase of the barrier length resulted in minor increases in area afflux suggesting that distribution of the logs in the YZ plane is more efficient for blocking the flow and storing the water upstream of the barrier than increased blockage in the longitudinal direction.

For the non-porous leaky barrier structures, the length of the barrier played a more noticeable role together with the cross-sectional blockage of the main channel. With no

263 flow through the voids of the leaky barrier, the area afflux was twice that of porous barriers.
264 This effect was accentuated by increase in the blockage ratio of the barrier, where increase
265 in the number of logs in the vertical plane, and therefore H_s led to large increases in area
266 afflux. Area afflux ranged between 0 and 15% for the porous barrier, and 0 to 28% for the
267 non-porous barrier. This highlights how accumulation of debris, sediment and smaller
268 branches may saturate the barrier, with flood attenuation performance improving as the
269 barrier matures. The spread of area afflux values for the same A_B (Figs. 7C and D) was due
270 to the differences in streamwise length of the barriers with similar barrier wood area and
271 blockage ratios. Again, changes in area afflux due to the streamwise blockage were evident,
272 however not as noticeable as the area afflux due to the cross-sectional flow blockage ratio.
273 This indicates that increases in wood volume and solid volume fraction are most beneficial
274 for flood attenuation when the wood pieces are arranged in a manner that maximises the
275 channel cross-section blockage area. The 80% bankfull discharge ($0.8Q_{bk}$) often resulted in
276 higher area afflux than the 100% bankfull discharge (Q_{bk}). This is attributed to area afflux
277 being normalised relative to the flow area associated with uniform flow condition, which
278 was lower for $0.8Q_{bk}$ than Q_{bk}, resulting in a greater proportional increase in area afflux for
279 the lower discharge condition compared to the higher discharge condition. Furthermore, the
280 increase in flow area in overbank flooding cases relates to the upstream flow spilling onto
281 the floodplain, which occurred more often for Q_{bk} than $0.8Q_{bk}$, inducing greater skin
282 friction losses and main channel/floodplain momentum exchange losses. Results here
283 indicate that the relative change in upstream flow area compared to the uniform flow
284 condition due to the leaky barrier's presence, is caused by hydraulic resistance in addition
285 to compound channel flow processes.

3.4. Effect of leaky barrier frontal projected area and orientation of logs on area afflux

To examine how complexity of the arrangement and distribution of logs affected flood attenuation performance, Linear, Lattice and Alternating configurations were compared (Fig. 8). These three configurations had similar volume of wood. More complex, i.e. less uniformly distributed log arrangements, of Lattice and Alternating barriers resulted in increased cross-sectional blockage area, but similar head loss compared to the geometrically arranged Linear barriers (see Fig. 2). As the barrier becomes longer, at higher blockage ratio this effect is more pronounced. For overbank flows, the Alternating barrier had overall lower area afflux than Linear for the bankfull discharge despite having a higher blockage ratio.

4. Discussion

The hydraulic effects of various designs of porous and non-porous engineered leaky barriers were studied by varying their physical characteristics of longitudinal length, blockage ratio, mode of formation and log arrangement. Overall, stage and area afflux increased with increasing leaky barrier longitudinal length and flow blockage ratio. However, unless accompanied by increases in barrier cross-sectional blockage area, increase in the barrier's length resulted in minor increases in stage and area afflux and head loss. Furthermore, our results highlighted that the cross-sectional flow blockage of the main channel (YZ plane) is a more important parameter than channel blockage in the longitudinal direction (XY plane) as area afflux was highest for arrangements where H_s, A_p and A_B were highest for both porous and non-porous barriers. The flow attenuation performance of the leaky barrier was dependent on cross-sectional blockage ratio of the flow or the projected

309 area of the barrier, and the distribution of logs, the mode of formation of the barrier, and the
310 height of the leaky barrier in the water column.
311 Alternating and Lattice barrier configurations use different angles of orientations, making
312 them more physically complex than the uniformly distributed arrays of the Linear
313 configuration. These complex barriers resulted in area afflux less than or equal to the area
314 afflux of Linear barriers. This suggests that barrier complexity is not necessarily an
315 indicator of improved flood attenuation, since Linear barriers result in similar, if not
316 greater, area afflux than more complex barriers, provided that length and blockage ratio
317 were maximised. Hence, it might be most beneficial in the design of engineered leaky
318 barriers to distribute logs in such a way that the greatest cross-sectional blockage area (YZ
319 plane) is achieved, maximising A_B and consequently area afflux and head loss. As barriers
320 mature and becomes more water-tight, with limited flow through due to the accumulation
321 of branches, leaves and sediments (Wallerstein and Thorne 1997; Manners et al. 2007;
322 Thomas and Nisbet 2012; Schalko et al. 2018), their attenuation performance will improve
323 and differences amongst different barrier designs will likely converge.
324 Flow depth and velocity differences between the main channel and floodplains contribute to
325 momentum exchange and friction losses for overbank flows (Knight and Demetriou 1983;
326 Shiono and Knight 1991). Additionally, higher flow depth ratio between the main channel
327 and floodplain, results in a higher ratio of the respective friction factors (Shiono and
328 Knight, 1991). However, observed variations in afflux for 80% and 100% bankfull
329 discharges were attributed to the leaky barrier presence contributing more to the increase in
330 flow area relative to initial uniform flow conditions than the friction and momentum
331 exchange for overbank flow, which occurred more frequently in the 100% bankfull cases.
332 Measurements of the hydrodynamic flow field in the presence of leaky barrier could further
333 explain this phenomenon.

334 The backwater effect and increased upstream flow depth implies decreased local velocities,
335 which would be favourable to fish seeking refuge areas (Wallerstein and Thorne 1997;
336 Shields et al. 2004; Manners and Doyle 2008; Floyd et al. 2009). Although a vertical gap
337 was left below the barrier for base flow and the free passage of fish, the flow through this
338 gap will likely be high due to the flow acceleration induced by the cross-sectional
339 constriction of the barrier and hence might form a velocity barrier to fish during high
340 discharge flood events (Castro-Santos 2005). This flow acceleration is also likely to result
341 in high shear stresses, which will exacerbate local scour on the channel bed below and
342 immediately downstream of the barrier, and the subsequent changes in bed level might
343 influence runoff attenuation of the barrier (Abbe and Montgomery 1996; Wallerstein and
344 Thorne 1997; Manners et al. 2007; Quinn et al. 2013; Schalko et al. 2019). In addition to
345 water quality benefits from trapping sediments and pollutants, such geomorphological
346 effects of leaky barriers are postulated to enhance fish habitat heterogeneity and their
347 creation might result in ecosystem services benefits by providing refuge areas and trapping
348 nutrients (Abbe and Montgomery 1996; Floyd et al. 2009; Dadson et al. 2017; Burgess-
349 Gamble et al. 2017; SEPA 2015).
350 Leaky barrier failures may contribute to wood load transport in the channels, which can
351 result in increased blockage and flood risk downstream, particularly during flood events
352 (Thomas and Nisbet 2012; Burgess-Gamble et al. 2017). Use of anchoring methods to
353 ensure the longterm stability of leaky barriers can alleviate this issue (D'Aoust and Millar
354 2000; Shields et al. 2004); although further research regarding the design, structural
355 integrity and failure risk posed by leaky barriers is necessary and recommended.
356 For flood modelling applications, a relationship between discharge, leaky barrier
357 characteristics and area afflux rise could be established using experimental or numerical
358 methods, based on the findings shown in the current experiments regarding the parameters

359 which maximise area afflux rise and flood attenuation for leaky barriers. The backwater
360 effect, floodplain water storage and increased infiltration directly alter groundwater table
361 and therefore affecting flood routing outcomes. Furthermore, in a catchment-based
362 approach, evaluating series of multiple leaky barriers on a channel and their cumulative
363 flood attenuation effect could provide further understanding of the potential and practice of
364 using leaky barriers in NFM.

365 **5. Conclusions**

366 The hydraulics of flood attenuation performance of leaky barriers were studied by
367 evaluating the backwater effects of different leaky barrier designs under 80% and 100%
368 bankfull flow conditions. Leaky barrier designs varied by physical characteristics of
369 streamwise length, cross-sectional blockage ratio, and mode of formation and distribution
370 of components in arrays of horizontal or inclined members. Cross-sectional blockage ratio
371 governed stage and area afflux, and hydrodynamic drag more than the blockage in the
372 longitudinal direction for all array configurations of leaky barriers. Linear non-porous
373 barriers with highest blockage ratio, also showed greater increases in area afflux with
374 increasing leaky barrier longitudinal length than other linear leaky barrier cases. Non-
375 porous representations of leaky barrier showed at least twice the area afflux compared to
376 porous barriers, indicating that as the engineered barriers become more watertight through
377 the accumulation of organic matter and debris, their flood attenuation performance will
378 improve. However, for inbank flows, head loss and stage afflux were positively correlated
379 with the wood volume composing the leaky barrier. The cross-sectional blockage ratio of
380 the channel occupied by the barrier was the most primary factor that influenced area afflux,
381 and hence, distributing logs to maximize channel obstruction will improve flood
382 attenuation.

Acknowledgments

The authors do not have any conflicts of interest. This work was supported by a Cardiff University International PhD studentship to VM.

References

Abbe, T.B., Montgomery, D.R., 1996. Large woody debris jams, channel hydraulics and habitat formation in large rivers. *Regul. Rivers Res. Manag*. 12, 201–221.

Burgess-Gamble, L., Ngai, R., Wilkinson, M., Nisbet, T., Pontee, N., Harvey, R., Kipling, K., Addy, S., Rose, S., Maslen, S., 2017. *Working with Natural Processes – Evidence Directory*.

Carrera, L., Standardi, G., Bosello, F., Mysiak, J., 2015. Assessing direct and indirect economic impacts of a flood event through the integration of spatial and computable general equilibrium modelling. *Environ. Model. Softw*. 63, 109–122. https://doi.org/10.1016/j.envsoft.2014.09.016

Castro-Santos, T., 2005. Optimal swim speeds for traversing velocity barriers: an analysis of volitional high-speed swimming behavior of migratory fishes. *J. Exp. Biol.* 208, 421–432.

Chow, V. Te, 1959. *Open-Channel Hydraulics*. International. Ed. McGraw-Hill Book Company, Inc., New York. 680 p.

Dadson, S.J., Hall, J.W., Murgatroyd, A., Acreman, M., Bates, P., Beven, K., Heathwaite, L., Holden, J., Holman, I.P., Lane, S.N., O'Connell, E., Penning-Rowsell, E., Reynard, N., Sear, D., Thorne, C., Wilby, R., 2017. A restatement of the natural science evidence concerning catchment-based 'natural' flood management in the UK. *Proc. R.*

Soc. A Math. Phys. Eng. Sci. 473, 20160706. https://doi.org/10.1098/rspa.2016.0706

Daniels, M.D., Rhoads, B.L., 2007. Influence of experimental removal of large woody debris on spatial patterns of three-dimensional flow in a meander bend. *Earth Surf. Process. Landforms.* 32, 460–474. https://doi.org/10.1002/esp

D'Aoust, S. G., and Millar, R. G., 2000. Stability of ballasted woody debris habitat structures." *J. Hydraul. Eng.* 126 (11), 810–817. https://doi.org/10.1061/(ASCE)0733-9429(2000)126:11(810)

Dixon, S.J., Sear, D.A., 2014. The influence of geomorphology on large wood dynamics in a low gradient headwater stream. *Water Resour. Res.* 50, 9194–9210. https://doi.org/10.1002/2014WR015947

Dodd, J.A., Newton, M & Adams, C.E. 2016. The effect of natural flood management in-stream wood placements on fish movement in Scotland, CD2015_02. Centre for Expertise in Water (CREW), Aberdeen, Scotland.

Fleming, G., 2002. Learning to live with rivers—The ICE's report to government, in: *Proceedings of the Institution of Civil Engineers-Civil Engineering.* Thomas Telford Ltd, pp. 15–21.

Floyd, T.A., MacInnis, C., Taylor, B.R., 2009. Effects of artificial woody structures on Atlantic salmon habitat and populations in a Nova Scotia stream. *River Res. Appl.* 25, 272–282. https://doi.org/10.1002/rra.1154

Gippel, C.J., 1995. Environmental Hydraulics of Large Woody Debris in Streams and Rivers. *J. Environ. Eng*. 121, 388–395. https://doi.org/10.1061/(ASCE)0733-9372(1995)121:5(388)

Gippel, C.J., Finlayson, B.L., O'Neill, I.C., 1996a. Distribution and hydraulic significance of large woody debris in a lowland Australian river. *Hydrobiologia* 318, 179–194. https://doi.org/10.1007/BF00016679

Gippel, C.J., Finlayson, B.L., O'Neill, I.C., 1992. *The hydraulic basis of snag management.* Centre for Environmental Applied Hydrology, Department of Civil and Agricultural Engineering, University of Melbourne.

Gippel, C.J., O'Neill, I.C., Finlayson, B.L., Schnatz, I., 1996. Hydraulic Guidelines for the Re-Introduction and Management of Large Woody Debris in Lowland Rivers. *Regul. Rivers Res. Manag.* 12, 223–236.

Giriat, D., Gorczyca, E., Sobucki, M., 2016. Beaver ponds' impact on fluvial processes (Beskid Niski Mts., SE Poland). *Sci. Total Environ.* 544, 339–353. https://doi.org/10.1016/j.scitotenv.2015.11.103

Gregory, K.J., Gurnell, A.M., Hill, C.T., 1985. The permanence of debris dams related to river channel processes. *Hydrol. Sci. J.* 30, 371–381. https://doi.org/10.1080/02626668509491000

Kitts, D., 2010. *The hydraulic and hydrological performance of large wood accumulation in a low-order forest stream.* Unpublished PhD dissertation, University of Southampton.

Knight, D.W., Demetriou, J.D., 1983. Flood Plain and Main Channel Flow Interaction. *J. Hydraul. Eng.* 109, 1073–1092. https://doi.org/10.1061/(ASCE)0733-9429(1983)109:8(1073)

Manners, R.B., Doyle, M.W., 2008. A mechanistic model of woody debris jam evolution and its application to wood-based restoration and management. *River Res. Appl.* 24, 1104–1123. https://doi.org/10.1002/rra.1108

Manners, R.B., Doyle, M.W., Small, M.J., 2007. Structure and hydraulics of natural woody debris jams. *Water Resour. Res.* 43, 1–17. https://doi.org/10.1029/2006WR004910

Nisbet, T.R., Marrington, S., Thomas, H., Broadmeadow, S., Valatin, G., 2011. *Slowing the flow at Pickering*. Final Report to Defra, Project RMP5455.

457 Nyssen, J., Pontzeele, J., Billi, P., 2011. Effect of beaver dams on the hydrology of small
458 mountain streams: Example from the Chevral in the Ourthe Orientale basin, Ardennes,
459 Belgium. *J. Hydrol.* 402, 92–102. https://doi.org/10.1016/j.jhydrol.2011.03.008
460 Odoni, N.A., Lane, S.N., 2010. Assessment of the Impact of Upstream Land Management
461 Measures on Flood Flows in Pickering Beck Using Overflow. *Project RMP55455:*
462 *Slowing the flow at Pickering.*
463 Pellicani, R., Parisi, A., Iemmolo, G., Apollonio, C., 2018. Economic Risk Evaluation in
464 Urban Flooding and Instability-Prone Areas: The Case Study of San Giovanni
465 Rotondo (Southern Italy). *Geosciences* 8, 112.
466 https://doi.org/10.3390/geosciences8040112
467 Pitt, M., 2008. *Learning lessons from the 2007 floods.* Cabinet Office London.
468 Puttock, A., Graham, H.A., Cunliffe, A.M., Elliott, M., Brazier, R.E., 2017. Eurasian
469 beaver activity increases water storage, attenuates flow and mitigates diffuse pollution
470 from intensively-managed grasslands. *Sci. Total Environ.* 576, 430–443.
471 https://doi.org/10.1016/j.scitotenv.2016.10.122
472 Quinn, P., O'Donnell, G., Nicholson, A., Wilkinson, M., Owen, G., Jonczyk, J., Barber, N.,
473 Hardwick, M., Davies, G., 2013. Potential Use of Runoff Attenuation Features in
474 Small Rural Catchments for Flood Mitigation. *Newcastle University, Environment*
475 *Agency, Royal Haskoning DHV, England.*
476 Ranga Raju, K.G., Rana, O.P.S., Asawa, G.L., Pillai, A.S.N., 1983. Rational assessment of
477 blockage effect in channel flow past smooth circular cylinders. *J. Hydraul. Res.* 21,
478 289–302. https://doi.org/10.1080/00221688309499435
479 Roni, P., Beechie, T., Pess, G., Hanson, K., 2015. Wood placement in river restoration:
480 fact, fiction, and future direction. *Can. J. Fish. Aquat. Sci.* 72, 466–478.
481 https://doi.org/10.1139/cjfas-2014-0344

Schalko, I., Schmocker, L., Weitbrecht, V., Boes, R.M., 2018. Backwater Rise due to Large Wood Accumulations. *J. Hydraul. Eng.* 144, 04018056. https://doi.org/10.1061/(ASCE)HY.1943-7900.0001501

Schalko, I., Lageder, C., Schmocker, L., Weitbrecht, V., Boes, R.M., 2019. Laboratory flume experiments on the formation of spanwise large wood accumulations: I. Effect on backwater rise. Water Resour. Res. 55, 2018WR024649. https://doi.org/10.1029/2018WR024649

SEPA, 2015. *Natural Flood Management Handbook*. Scottish Environment Protection Agency (SEPA) Stirling.

Shields, F.D., Morin, N., Cooper, C.M., 2004. Large Woody Debris Structures for Sand-Bed Channels. *J. Hydraul. Eng.* 130, 208–217. https://doi.org/10.1061/(ASCE)0733-9429(2004)130:3(208)

Shields, F.D.J., Gippel, C.J., 1995. Prediction of Effects of Woody Debris Removal on Flow Resistance. *J. Hydraul. Eng.* 121, 341–354.

Shiono, K., Knight, D.W., 1991. Turbulent open-channel flows with variable depth across the channel. *J. Fluid Mech.* 222, 617–646. https://doi.org/10.1017/S0022112091001246

Thomas, H., Nisbet, T., 2012. Modelling the hydraulic impact of reintroducing large woody debris into watercourses. *J. Flood Risk Manag.* 5, 164–174. https://doi.org/10.1111/j.1753-318X.2012.01137.x

UNISDR (2015). *Making Development Sustainable: The Future of Disaster Risk Management. Global Assessment Report on Disaster Risk Reduction*. Geneva, Switzerland: United Nations Office for Disaster Risk Reduction (UNISDR).

Wallerstein, N., Thorne, C.R., 1997. *Impacts of woody debris on fluvial processes and channel morphology in stable and unstable streams*. Nottingham Univ (United

507 Kingdom), Dept of Geography.
508 Wenzel, R., Reinhardt-Imjela, C., Schulte, A., Bölscher, J., 2014. The potential of in-
509 channel large woody debris in transforming discharge hydrographs in headwater areas
510 (Ore Mountains, Southeastern Germany). *Ecol. Eng.* 71, 1–9.
511 https://doi.org/10.1016/j.ecoleng.2014.07.004
512 Wohl, E., 2013. Floodplains and wood. *Earth-Science Rev.* 123, 194–212.
513 https://doi.org/10.1016/j.earscirev.2013.04.009
514 Young, W.J., 1991. Flume study of the hydraulic effects of large woody debris in lowland
515 rivers. *Regul. Rivers Res. Manag*. 6, 203–211.

516 **Figure captions**

517 Fig. 1. Diagram illustrating the flow attenuation process of leaky barriers where flow is
518 temporally stored upstream of the barrier, spilling onto floodplains and increasing ground
519 water infiltration and the resulting reduction of downstream flow depths.

520 Fig. 2. Diagrams of leaky barrier configurations, geometry and arrangements showing (A)
521 longitudinal elevation view of the experimental setup, (B) cross-sectional view of the
522 symmetrical compound open channel, and Linear (test series A) configuration, which is
523 shown as longitudinal elevation in (C). (D) and (E) show the distribution of logs
524 comprising the Alternating (test series C) configuration. A gap (b_0) was maintained
525 between the lowest log of the barrier and the flume bed to allow potential fish passage. The
526 dotted and dashed lines circles in (A) indicate the direction of removal of the logs as the
527 barrier was deconstructed from 8**Di* (200mm) to 1**Di* (25 mm). L_x denotes the length of
528 the barrier in the longitudinal direction. Diagrams not to scale.

529 Fig. 3. Longitudinal surface water profiles: flow depth *h* (mm) relative to longitudinal
530 distance X(m) for the 'Linear' (H_s=95mm) (test series A24 and A48) with longitudinal
531 length L_x= 200 mm for the 100% bankfull Q_{bk} discharge. The grey rectangular shape
532 outlines the location of the non-porous barrier. Flow direction is from left to right.

533 Fig. 4. Effect of 'Linear' (test series A), 'Lattice'(test series B), and 'Alternating' (test
534 series C) leaky barrier design on head loss h_L, showing the performance of a similar
535 longitudinal lengths L_x/D_i (A), and flow blockage ratios A_B (B). All data points shown here
536 are for the porous barrier setup with inbank flows. These show effect of configuration,
537 geometry, angle of orientation and arrangement, as well as the resulting projected areas and
538 blockage ratios on the performance of the leaky barrier.

539 Fig. 5. Stage afflux of Linear porous leaky barriers with Hs = 60 and 95 mm and L_x/D_i = 4,
540 5, 6, 7 and 8 with inbank flows under 80% and 100% bankfull discharges (0.8Q_{bk} and Q_{bk},
541 respectively). From Schalko et al. (2019), based on Froude number similar to the current
542 experiments, Series A7 with Fr = 0.30 (Q = 11 Ls^{-1}, h_o=100 mm, U_0 = 0.30 ms^{-1}) was
543 chosen for comparison. Δh is the stage afflux upstream of the barrier, shown relative to the
544 uniform flow depth h_0. V_s is the solid volume of wood and B_{mc} is the main channel width.

545 Fig. 6. (A) Drag coefficient (C_D) of leaky barrier in relation to non-dimensional
546 longitudinal length (L_x/D_i) for porous and non-porous Linear dams with inbank flows,
547 showing the variation of drag coefficient with L_x/D_i for the 80% bankfull discharge. H_s =
548 25, 60, and 95 mm correspond to the barrier height. (B) Variation of C_D values with
549 blockage ratio in comparison to literature data which used large wood as presented in
550 Shields and Alonso (2012).

551 Fig. 7. Effect of barrier streamwise length L_x/D_i (A and B), the cross-sectional flow
552 blockage ratio due to the barrier A_B (-) (C and D) on area afflux (100x $\Delta A/A_0$) for barrier
553 heights H_s =25, 60 and 95 mm for the 'Linear' barrier configurations under 80% and 100%
554 bankfull discharges (0.8Q_{bk} and Q_{bk}, respectively). Standard error for flow area afflux was
555 0.7% and 1.5% for porous (A and C) and non-porous (B and D) barriers, respectively.

556 Fig. 8. Comparison of area afflux (100x $\Delta A/A_0$) for porous Linear (series A1-A24), Lattice
557 (test series B1-B8) and Alternating (Series C1-C8) configurations under 80% and 100%
558 bankfull discharges (0.8Q_{bk} and Q_{bk}, respectively) for specific barrier lengths L_x/D_i =1 to 8.

559

560

561 Figure 1.

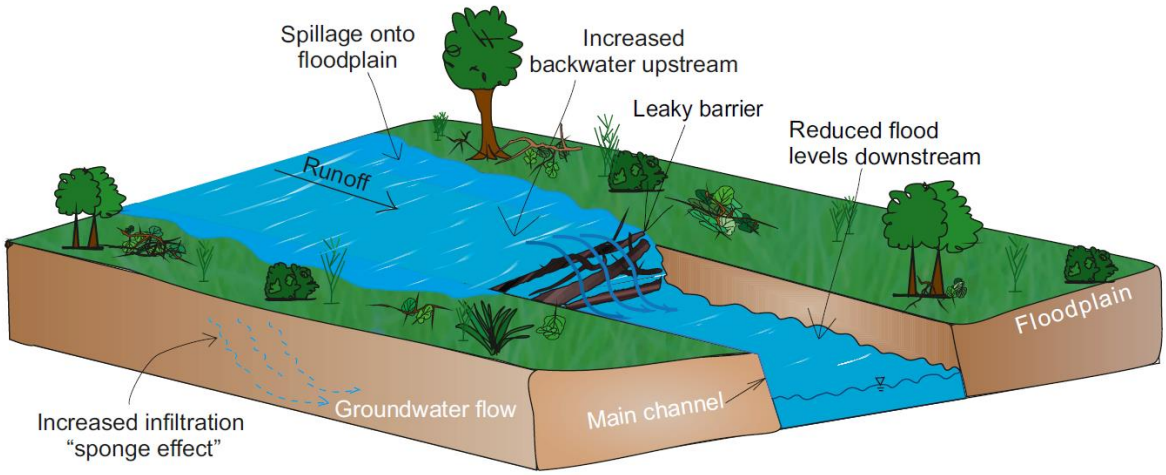

562

563 Figure 2.

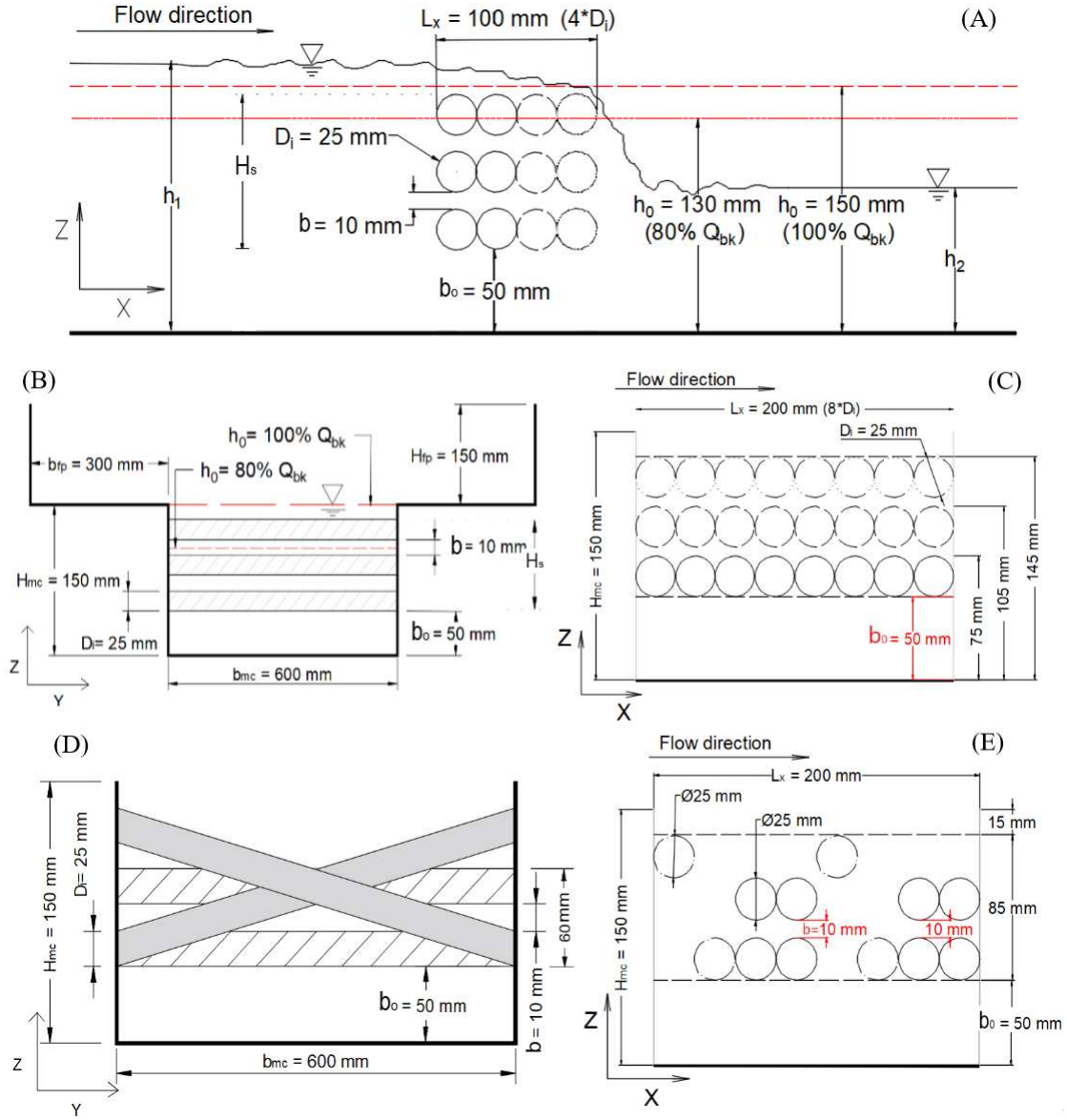

564

Figure 3.

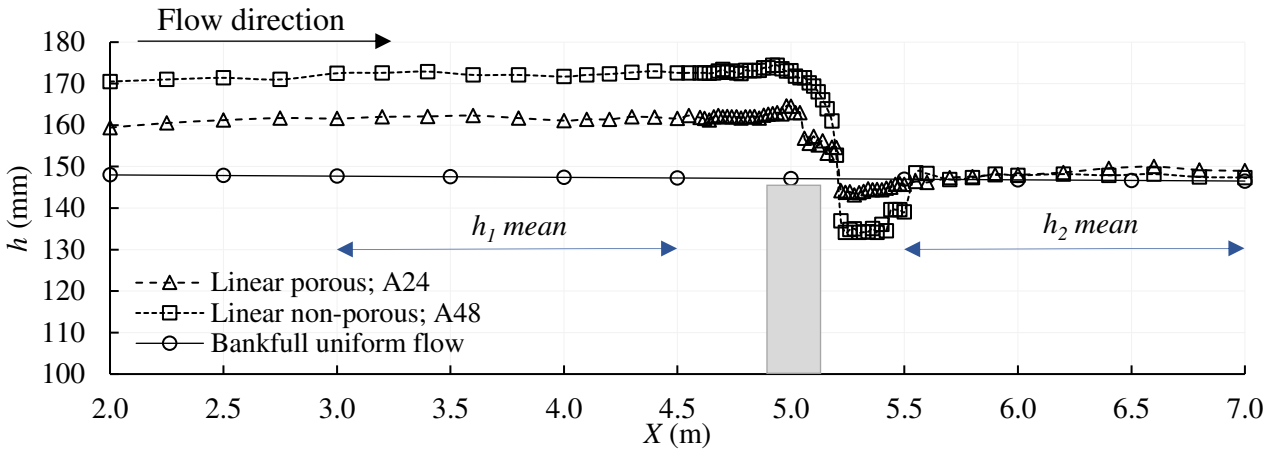
Flow direction
180
170
160
150
140
130
120
110
100
h (mm)
h1 mean
h2 mean
Linear porous; A24
Linear non-porous; A48
Bankfull uniform flow
2.0
2.5
3.0
3.5
4.0
4.5
5.0
5.5
6.0
6.5
7.0
X (m)

Figure 4.

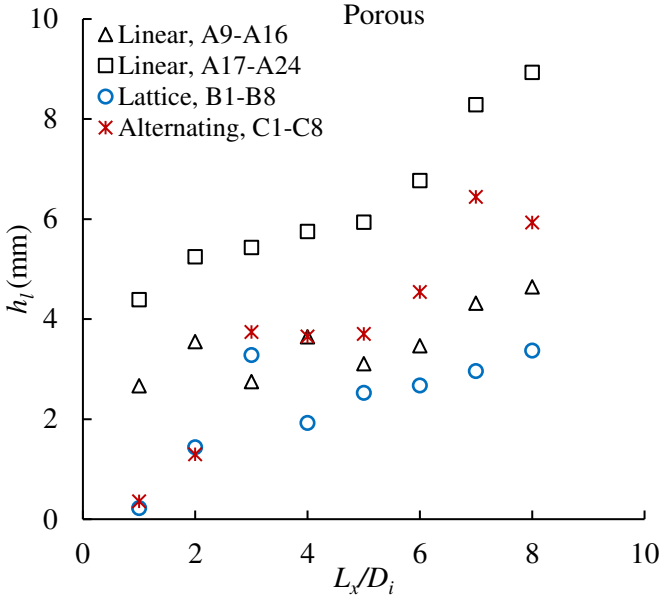
Porous
Linear, A9-A16
Linear, A17-A24
Lattice, B1-B8
Alternating, C1-C8
h_l (mm)
L_x/D_i
0
2
4
6
8
10

(A)

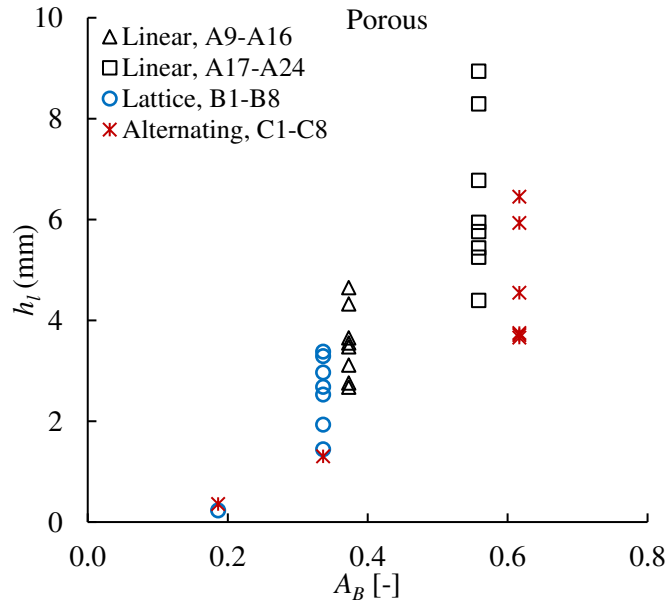
Porous
Linear, A9-A16
Linear, A17-A24
Lattice, B1-B8
Alternating, C1-C8
h_l (mm)
A_B [-]
0
2
4
6
8
10
0.0
0.2
0.4
0.6
0.8

(B)

Figure 5.

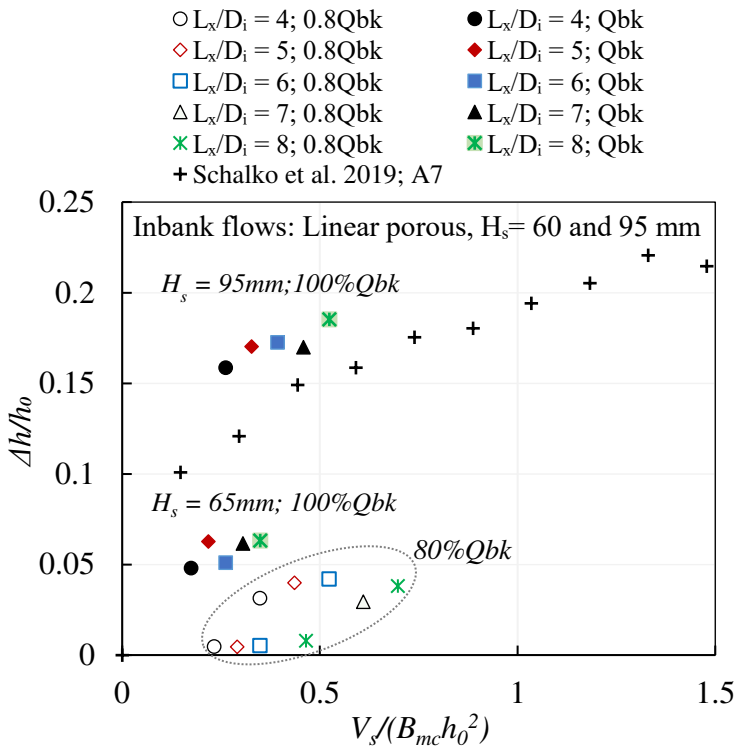
○ Lx/Di = 4; 0.8Qbk
● Lx/Di = 4; Qbk
◇ Lx/Di = 5; 0.8Qbk
◆ Lx/Di = 5; Qbk
□ Lx/Di = 6; 0.8Qbk
■ Lx/Di = 6; Qbk
△ Lx/Di = 7; 0.8Qbk
▲ Lx/Di = 7; Qbk
✳ Lx/Di = 8; 0.8Qbk
✳ Lx/Di = 8; Qbk
+ Schalko et al. 2019; A7
Inbank flows: Linear porous, Hs= 60 and 95 mm
Hs = 95mm;100%Qbk
Hs = 65mm; 100%Qbk
80%Qbk
Δh/h0
Vs/(Bmch0²)
0.25
0.2
0.15
0.1
0.05
0
0
0.5
1
1.5

595 Figure 6.

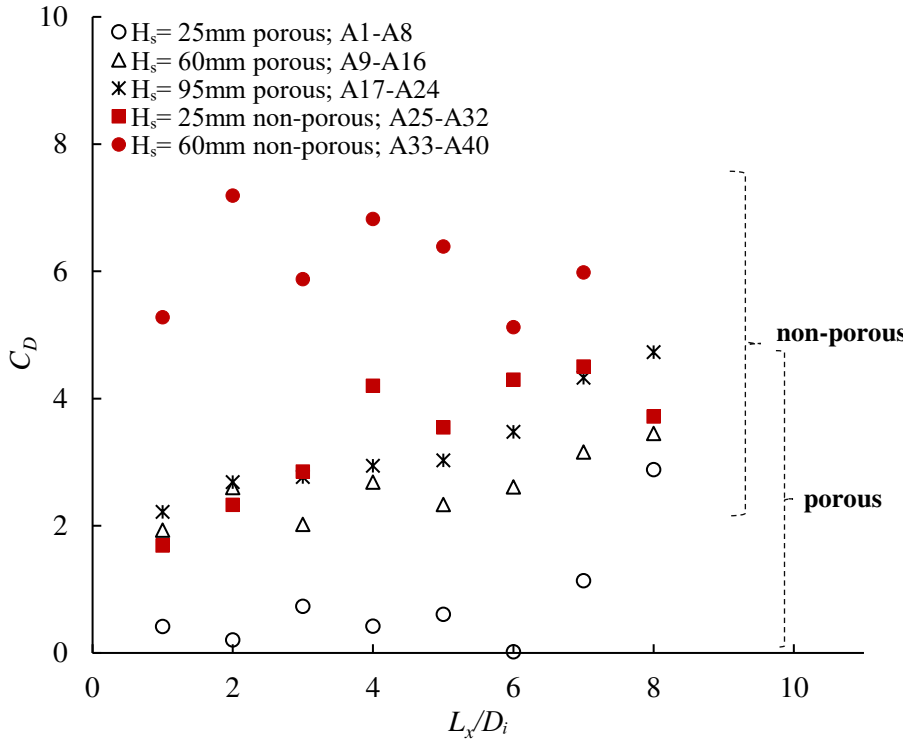

(A)

596

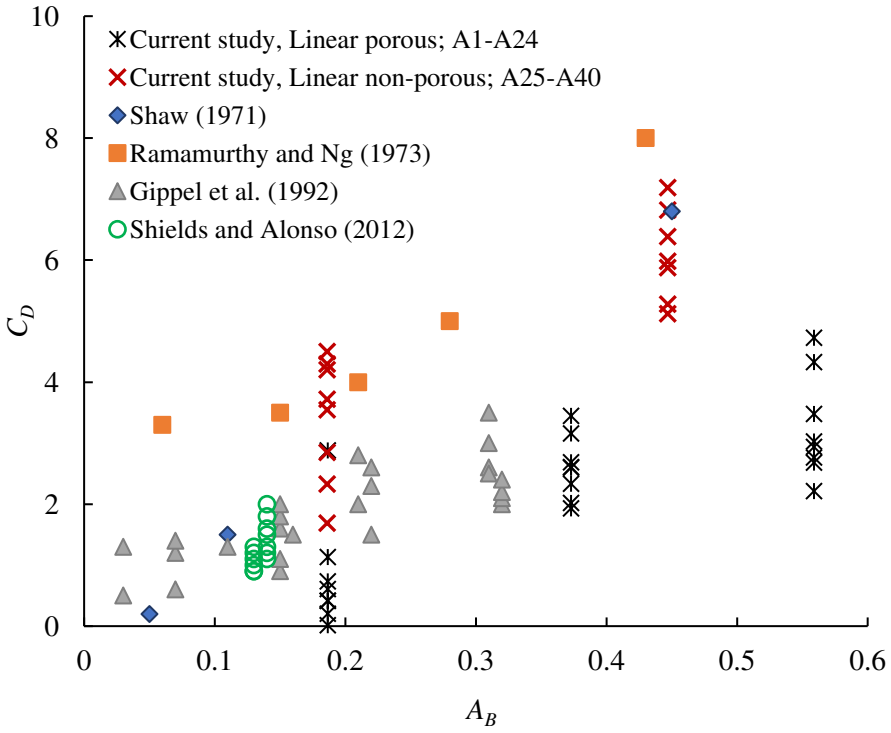

(B)

597

598 Figure 7.

599

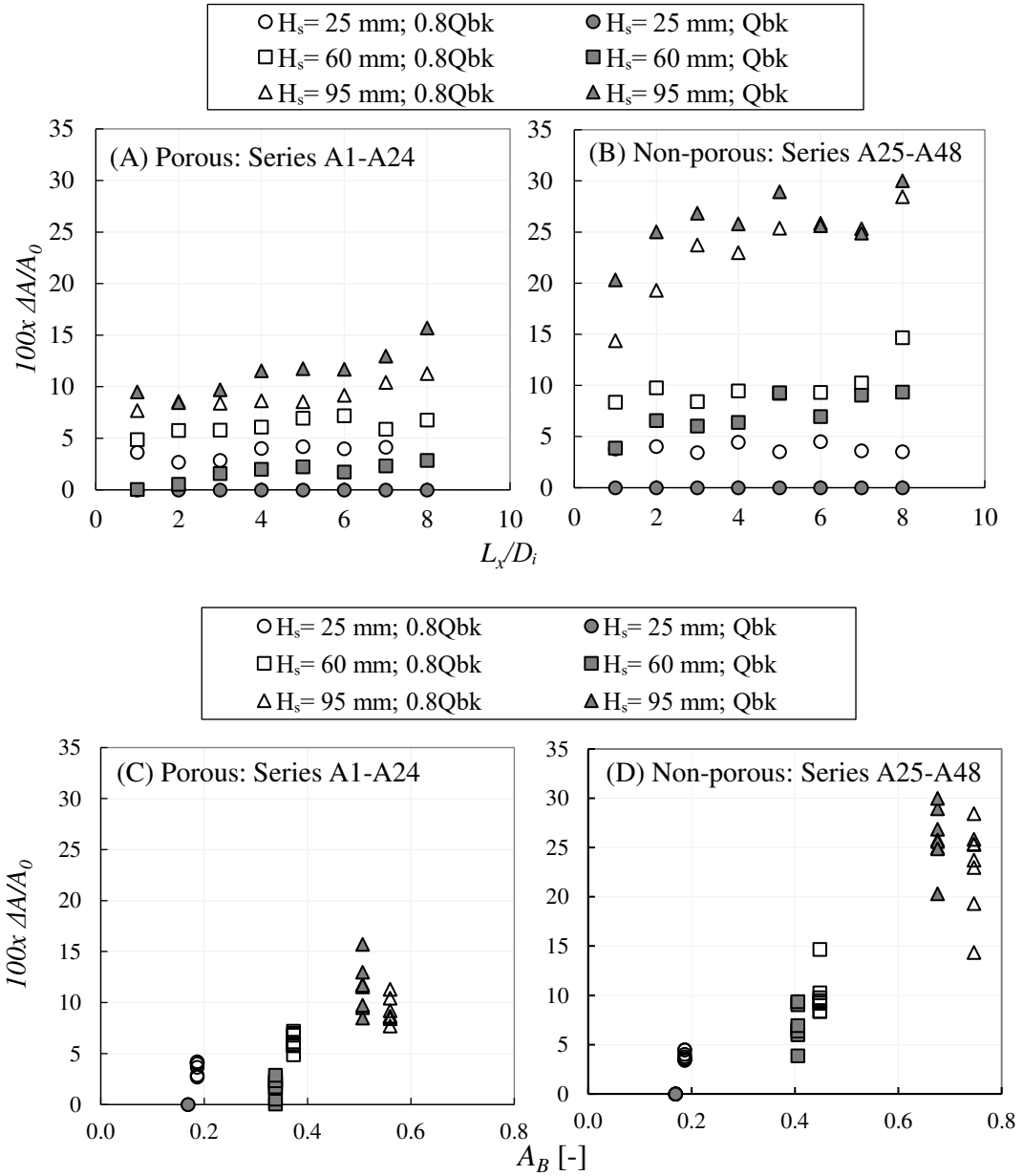

600

601

602

603

604

605

606

607

608

609

610

611

612 Figure 8.

613

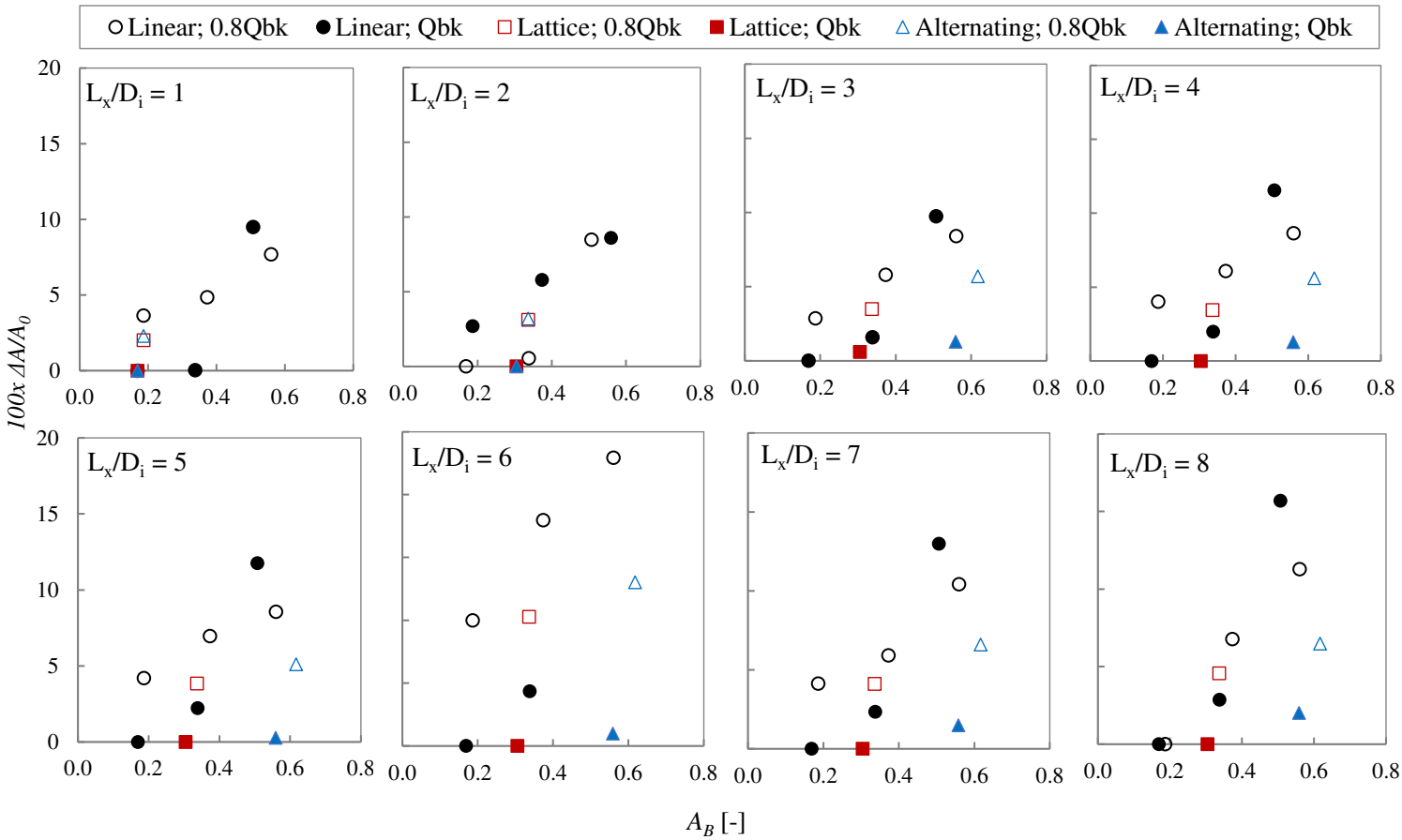

614

615 **Table caption**

616 Table 1. Test programme for Series A, B and C. All leaky barriers began at 5 m
617 downstream from the flume inlet. For all arrangements, there are no gaps between the logs
618 in the longitudinal flow direction. A vertical gap, b_0, of 50 mm was maintained for all tests.
619 Illustrations of A17-A24 and C1-C8 are shown in Figs. 2B and C, and Figs. 2D and E,
620 respectively. The uniform flow discharges of 22 and 28 Ls^{-1} correspond to Reynolds
621 numbers of 25,600 and 31,100, respectively.

Test series	Arrangement	Test effect	Q [Ls^{-1}]	Fr_0 [-]	h_0 [mm]	Hs [mm]	L_x [mm]	i [-]	Di [mm]	b_z [mm]
A1-A8	Linear	Porous	22, 28	0.29,0.31	130,150	25	25,50,75,100,125,150,175,200	1	25	10
A9-A16	Linear	Porous	22, 28	0.29,0.31	130,150	60	25,50,75,100,125,150,175,200	1	25	10
A17-A24	Linear	Porous	22, 28	0.29,0.31	130,150	95	25,50,75,100,125,150,175,200	1	25	10
A25-A32	Linear	Non-porous	22, 28	0.29,0.31	130,150	25	25,50,75,100,125,150,175,200	1	25	10
A33-A40	Linear	Non-porous	22, 28	0.29,0.31	130,150	60	25,50,75,100,125,150,175,200	1	25	10
A41-A48	Linear	Non-porous	22, 28	0.29,0.31	130,150	95	25,50,75,100,125,150,175,200	1	25	10
B1-B8	Lattice	Porous	22, 28	0.29,0.31	130,150	85	25,50,75,100,125,150,175,200	1	25	10
C1-C8	Alternating	Porous	22, 28	0.29,0.31	130,150	85	25,50,75,100,125,150,175,200	1	25	10

*For B1-B8 and C1-C8 this is the variation in barrier height in the cross-sectional flow area, see Fig 2(C)

622